Generation of picosecond pulsed coherent state superpositions

Dong, Ruifang; Tipsmark, Anders; Laghaout, Amine; Krivitsky, Leonid; Jezek, Miroslav; Andersen, Ulrik Lund

Published in:
Optical Society of America. Journal B: Optical Physics

Link to article, DOI:
10.1364/JOSAB.31.001192

Publication date:
2014

Document Version
Publisher's PDF, also known as Version of record

Generation of picosecond pulsed coherent state superpositions

Ruifang Dong,[1,2,5] Anders Tipsmark,[1] Amine Laghaout,[1] Leonid A. Krivitsky,[1,3] Miroslav Ježek,[1,4] and Ulrik Lund Andersen[1,6]

[1]*Department of Physics, Technical University of Denmark, Fysikvej, 2800 Kgs. Lyngby, Denmark*
[2]*Quantum Frequency Standards Division, National Time Service Center (NTSC), Chinese Academy of Sciences, 710600 Lintong, China*
[3]*Data Storage Institute, Agency for Science Technology and Research (A*STAR), 117608 Singapore*
[4]*Department of Optics, Palacký University, 17. listopadu 12, 77146 Olomouc, Czech Republic*
[5]*e-mail: dongruifang@ntsc.ac.cn*
[6]*e-mail: ulrik.andersen@fysik.dtu.dk*

Received January 7, 2014; revised March 1, 2014; accepted March 28, 2014;
posted March 28, 2014 (Doc. ID 203509); published April 28, 2014

We present the generation of approximated coherent state superpositions—referred to as Schrödinger cat states—by the process of subtracting single photons from picosecond pulsed squeezed states of light. The squeezed vacuum states are produced by spontaneous parametric down-conversion (SPDC) in a periodically poled $KTiOPO_4$ crystal while the single photons are probabilistically subtracted using a beamsplitter and a single photon detector. The resulting states are fully characterized with time-resolved homodyne quantum state tomography. Varying the pump power of the SPDC, we generated different states which exhibit non-Gaussian behavior.

OCIS codes: (270.0270) Quantum optics; (190.4410) Nonlinear optics, parametric processes; (270.6570) Squeezed states; (320.5390) Picosecond phenomena; (270.5585) Quantum information and processing.
http://dx.doi.org/10.1364/JOSAB.31.001192

1. INTRODUCTION

Quantum information processing solely based on Gaussian states and Gaussian operations is a largely matured field of research. The preparation of squeezed states—the ubiquitous resource in many Gaussian protocols—has experienced large progress in recent years. States with a high purity or a high degree of squeezing have been produced [1–4]. Moreover, Gaussian projectors can be implemented using homodyne detection, which is capable of reaching near-unity detection efficiency [1]. Finally, Gaussian displacement operations combined with low-noise linear feedback have been implemented with high quality [5–8]. This progress has lead to the implementation of various Gaussian protocols such as quantum teleportation [9], quantum key distribution [10], quantum cloning [11], quantum secret sharing [12], and quantum computation [13,14].

However, several no-go theorems exist for systems consisting of purely Gaussian states and Gaussian operations. With this constrained set of states and operations it is impossible to perform entanglement distillation [15–17], quantum error correction [18], universal quantum computing [19,20], quantum bit commitment [21], and to violate Bell's inequality [22]. To realize these protocols, non-Gaussian approaches are required. This non-Gaussianity can be injected into the system at different stages. It can enter through a non-Gaussian measurement strategy [23–25], non-Gaussian noise characteristics [26], or it can be incorporated through a non-Gaussian state preparation strategy [27–32].

Important examples of a pure non-Gaussian state are the photon number eigenstates, the Fock states $|n\rangle$, $(n = 1, 2\ldots)$. Such states have been prepared and fully characterized in optical systems using SPDC followed by a non-Gaussian heralding measurement [33–40]. Another family of non-Gaussian states, which has gained much interest in recent years, are the Schrödinger cat states which are superpositions of two coherent states of different phase, $|\alpha\rangle \pm |-\alpha\rangle$. Despite the constituents being Gaussian, the superposition exhibits strong non-Gaussianity which is sufficient for the realization of various protocols, examples being the realization of quantum information [41,42], quantum computation [27,43–46], error correction of Gaussian noise [30], and the violation of Bell's inequality [31,47–49].

It has been demonstrated that such coherent state superpositions (CSS) with a moderate amplitude $\alpha \lesssim 1$ can be well approximated by a photon-subtracted squeezed state [50,51], or equivalently, a squeezed single-photon state. Fidelities between the ideal CSS state and the photon-subtracted squeezed state as a function of the excitation, α, of the CSS and the degree of squeezing of the squeezed state are shown in Fig. 1. The moderate amplitude of the CSS can be nondeterministically amplified to a larger amplitude CSS by means of linear interference and heralding based on photon counting or homodyne detection events [28,52–54]. A large CSS can also be prepared through a conditional homodyne measurement on a Fock state in which the amplitude of the CSS state scales with the number of photons in the Fock state [55].

Inspired by these ideas for the generation of CSS and motivated by the potential applications, various groups have realized photon subtraction with squeezed states [55–61]. These implementations have been carried out either with

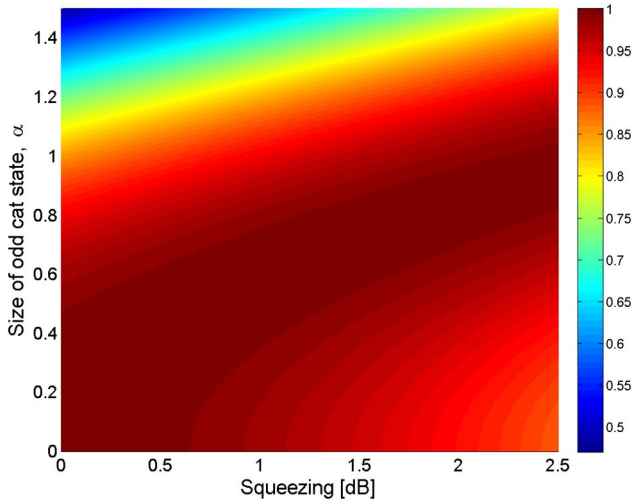

Fig. 1. Fidelity between a photon-subtracted squeezed state and an ideal coherent state superposition, $|\alpha\rangle - |-\alpha\rangle$, for different degrees of squeezing. It can be seen that the fidelity remains high, $F > 0.9$, for α up to 1, provided the squeezing degree is not too large.

continuous wave (CW) or pulsed light sources, and with wavelengths ranging from the near-infrared to the telecommunication regime. The photon subtraction has been carried out using an asymmetric beamsplitter that reflects a small portion of the light in which a photon is measured and thus subtracted from the squeezed state. The measurement has been realized with single-photon avalanche photodiodes (APD) as well as with photon-number-resolving transition edge sensors.

The largest directly measured value of the Wigner function negativity is −0.171 and it is obtained using CW squeezed states [62]. Using pulsed instead of CW squeezed light, the reported negativities as well as the purities of the generated non-Gaussian states are much lower. Despite the lower quality of the generated states, there has been much interest in pulsed experiments due to the relative simplicity of the experimental setup and the inherent temporal confinement of the generated states. Previous pulsed experiments on generating CSS with a negative Wigner function have employed femtosecond pulsed lasers [35,59]. In these experiments, the nonlinear crystal used for squeezed light generation was kept in the submillimeter range in order to avoid the detrimental effects of group velocity dispersion (GVD) and gain induced diffraction [63].

The advantage of picosecond over femtosecond pulses is that GVD is relatively reduced, making it possible to employ a longer nonlinear crystal. In addition, dispersion effects in the transmission line are also reduced. Namekata *et al.* have recently realized a non-Gaussian operation by using a 5 ps pulsed fiber laser at 1560 nm and a 3 mm long, periodically poled, lithium niobate waveguide. However, no negative values in the measured Wigner functions were observed due to the low overall efficiency of the experiment and the low modal purity of the generated states [60].

In this paper, we present the first experimental demonstration of CSS with a negative Wigner function in the ps-pulsed regime. Single photons are subtracted from squeezed vacuum states produced in a 3 mm long quasi-phase matched periodically poled $KTiOPO_4$ (PPKTP) crystal pumped by 4.6 ps laser pulses at 830 nm. The generated photon-subtracted squeezed vacuum states are measured and characterized with various squeezing factors. All the experimental results demonstrate strong non-Gaussian properties and the largest directly measured negativity was 0.023 without any loss-corrections.

2. EXPERIMENT

A CSS state with a small amplitude can be approximated by a photon-subtracted squeezed state, and it can be fully characterized by means of its Wigner function which is obtainable by homodyne tomography. In the following we present the different parts of our experimental setup to generate and characterize a CSS. We introduce the two required parametric processes (up-conversion and down-conversion), the photon-subtraction setup, and finally the homodyne detector. We also briefly discuss a simple model for predicting the performance of the experiment.

The experimental setup is shown in Fig. 2. We used a cavity-dumped titanium-sapphire pulsed laser (Tiger-PS, Time-Bandwidth Products), which produced nearly Fourier-transform-limited pulses with a duration of 4.6 ps at 830 nm with an average energy up to 40 nJ and a repetition rate of 815 kHz. With a WS6 HighFinesse wavelength meter, the center wavelength and its bandwidth of the pulses were measured to be 829.7 and 0.16 nm, respectively, corresponding to a spectral width of 70 GHz. A fraction of about 10% was used as a local oscillator (LO) for homodyne detection, a weak seed beam was directed to the parametric down-conversion process for alignment and the remaining part was directed to a frequency doubling process.

A. Frequency Doubling

For frequency doubling, a 3 mm long periodically poled KTP crystal (PPKTP1) was used. The crystal poling-period was chosen for first order quasi-phase-matching corresponding to a poling period of $\Lambda \sim 3.8$ μm with all fields polarized along the crystal's z axis. The length of the crystal was chosen to be 3 mm for a compromise between having a large interaction length and avoiding phase mismatch due to GVD.

The beam waist was set to $w_0 \sim 90$ μm, thus achieving a weak focusing condition with the depth-of-focus ($2z_0 \sim 60$ mm) being 20 times longer than the crystal length [64,65]. The second harmonic conversion efficiency, η, was investigated as a function of input power of the fundamental beam and the result is displayed in Fig. 3. A maximum frequency doubling efficiency of 32% was achieved for an incident average power of 33 mW. The spectral properties of the resulting frequency doubled light was investigated by a WS6 HighFinesse wavelength meter and it was measured to

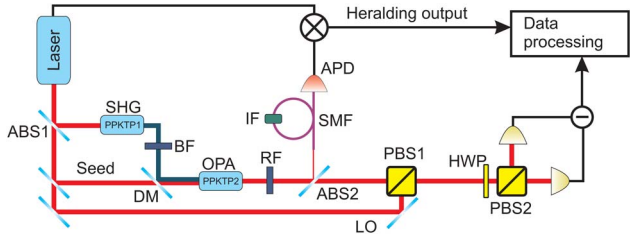

Fig. 2. Schematic of the experimental setup. The cavity dumped laser emits 4.6 ps optical pulses at 830 nm with a repetition frequency of 815 kHz. ABS1, 90/10 beamsplitter; BF, blue filter; DM, dichroic mirror; RF, red filter; ABS2, asymmetric beamsplitter with $R = 7.7\%$; SMF, single-mode fiber; IF, interference filter; APD, avalanche photodiode; PBS, polarizing beamsplitter; HWP, half-wave plate.

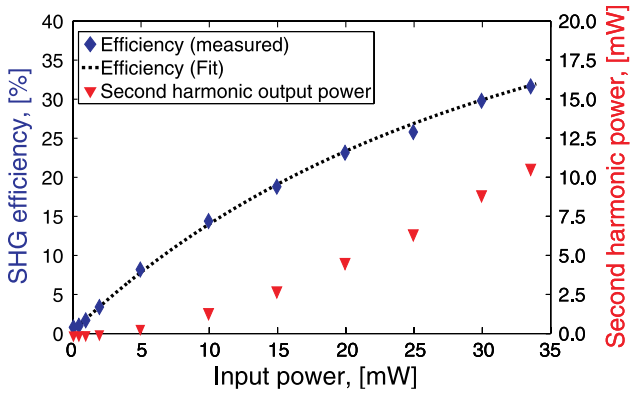

Fig. 3. (a) Blue diamonds correspond to the second-harmonic generation conversion efficiency for different input powers of the fundamental beam, P_F. These points are fitted with $\eta = \eta_\infty \tanh^2(g\sqrt{P_F})$, with $\eta_\infty = 0.53$ and $g = 0.18$. Red triangles are the total generated SHG power for different power levels of the fundamental beam.

have a center wavelength of 414.8 nm and a bandwidth of ~0.1 nm, corresponding to a spectral width of about 174 GHz.

B. Parametric Down-Conversion

After the frequency doubling crystal, the residual light at 830 nm was filtered out using a series of filters. The filtered blue light was then focused into a second PPKTP crystal (PPKTP2) used to generate a squeezed vacuum through the SPDC. It has been shown that for single pass pulsed SPDC experiments the gain-product $g_{\min}g_{\max}$, where $g_{\min}(g_{\max})$ is the attenuation (amplification) factor is enhanced by defocussing the pump [65,66]. This was confirmed in our setup, and the waist of the pump was set to $w_{0,p} \sim 150$ μm and a depth-of-focus of $2z_0 \sim 340$ mm. The pump can thus be regarded as a plane wave within the length of the crystal, leading to an improvement of the degree of squeezing [66]. After the SPDC, the remaining pump was filtered out using a series of filters. The generated squeezed vacuum was directed to an asymmetric beamsplitter (ABS2) with a reflectivity of $R \approx 7.7\%$. The reflected part was directed to an avalanche photodiode, while the transmitted part was subjected to full quantum state tomography by means of time-domain balanced homodyne detection (TD-BHD) [67,68].

In pulsed experiments, squeezing is often generated in a single pass configuration without the use of enhancement cavities. Thus the squeezing is generated in many different spatial and temporal modes [69–71]. The mode (and thus the degree of squeezing) being measured by the homodyne detector depends on the spatiotemporal profile of the LO: the mode of the squeezing spectrum that spatially and temporally overlaps with the LO will be measured by the homodyne detector. The amount of measured squeezing can be optimized by injecting a weak seed beam, corresponding to the mode of the LO, into the SPDC crystal and studying the classical parametric (de-)amplification of the seed beam. Depending on the relative phase between the seed and the pump, the seed can be either amplified or deamplified. Optimal phase-matching between the two waves is obtained for $w_{0,p}/w_{0,s} = \sqrt{2}$ [65], and thus we set the beam waist of the seed ($w_{0,s} =$ 106 μm). We achieved an optimal deamplification of $g_{\min} =$ 0.38 and an amplification of $g_{\max} = 4.6$ for a pump power

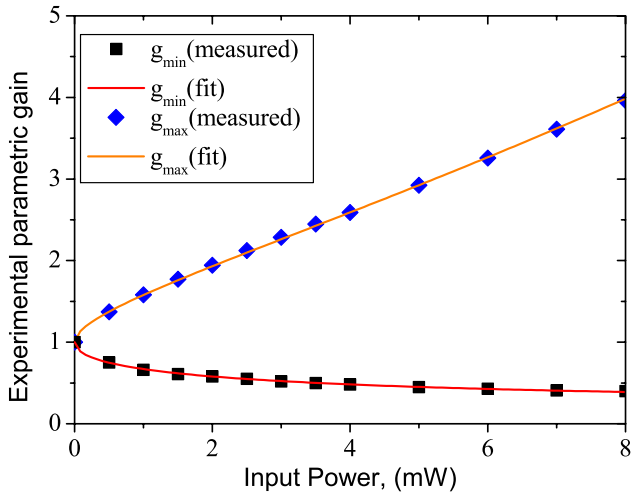

Fig. 4. Classical parametric gain versus average pump power, P_p. The squares correspond to the measured deamplification values, whereas the diamonds are the measured amplification values. The red and orange lines are fits using Eq. (1), with the intrinsic parametric gain $r = 0.28\sqrt{P_p(mW)}$ and $\varepsilon = 0.77 \pm 0.01$.

of 9 mW. A full characterization of the gains, $g_{\{\min,\max\}}$, as a function of pump power is shown in Fig. 4.

Using a simple model we find [72]

$$g_{\{\min,\max\}} = \varepsilon \exp(\{+2r, -2r\}) + (1 - \varepsilon), \quad (1)$$

where $\exp(\pm 2r)$ is the intrinsic gain and ε is a parameter describing the spatial overlap between the seed and the pump. ε was experimentally estimated to be 0.77 ± 0.01 (see below). Through power-shape fitting, the dependence of r on the pump power is found to be $r = 0.28\sqrt{P_p(\mathrm{mW})}$. This measurement of the classical gain also shows that within the gain range of our experiment, the effect of gain-induced diffraction is negligible [63,66].

C. Time-Domain Balanced Homodyne Detection

The measurement setup for homodyne detection is shown in Fig. 2. The transmitted squeezed vacuum state was superimposed with the LO at PBS1, the combined optical pulses were split at PBS2 and the resulting two beams were focused onto a pair of PIN photodiodes (Hamamatsu, S3883, quantum efficiency of $\eta_{\mathrm{ph}} = 0.95 \pm 0.02$). Using a HWP, the splitting ratio of PBS2 was tuned to balance the homodyne detector. The detector used in the experiment is based on the design by Hansen *et al.* [68]. Its output was recorded by a digital oscilloscope (LeCroy, LT374L) using the cavity dumper signal from the laser as a trigger. The final quadrature value is then extracted by integrating the signal over the individual pulses.

The integration requires a well-defined pulse window, T_w, which is determined by the repetition rate of the laser $f_{\mathrm{Rep}} =$ 815 kHz yielding $T_w \approx 1.2$ μs. The detector has a bandwidth of 2 MHz which is confirmed by the generation of 500 ns wide electronic pulses resulting from the detection of the picosecond optical pulses. Since electronic pulse is shorter than the pulse window, only a fraction of the pulse window contains valuable information. As a result, only a part of the measured pulse contributes to the integration, used to extract the quadrature values. We investigated the signal-to-noise ratio (SNR) (shot noise variance to electronic noise variance) of the

detection scheme for various choices of a weight function folded with the measured pulse. It was found that a simple boxcar-average, encompassing about 40% of the measurement window, was an optimal choice. The shot noise reference is obtained by measuring a vacuum input state. The reference level is known to increase linearly with the LO power. To verify that the system was indeed shot noise limited, we measured the shot noise as a function of the LO power, see Fig. 5(a). The electronic noise was measured to be 3.7 mV^2 which corresponds to 530 electrons/pulse. In Fig. 5(a), it is clearly seen that the shot noise depends linearly on the LO power, and the gain of the detector was found to be 13.6 $mV^2/10^6$ photons per pulse. In Fig. 5(b), the ratio between the shot noise and the electronic noise (electronic noise clearance) is plotted as a function of the LO power. It can be seen that the noise clearance surpasses 23 dB when the LO pulse contains more than 70×10^6 photons (corresponding to a power of ~12 μW). This corresponds to an electronic noise equivalent quantum efficiency of $\eta_{el} \geq 99.5 \pm 0.5\%$ [73].

The overall homodyne detection efficiency η_{hd} is given by

$$\eta_{\mathrm{hd}} = \eta_{\mathrm{op}}\eta_{\mathrm{mm}}^2\eta_{\mathrm{ph}}\eta_{\mathrm{el}}, \tag{2}$$

where η_{op} is the propagation efficiency of the state through optical components and η_{mm} is the degree of mode-matching between the LO and the squeezed pulse. These values were measured to be $\eta_{\mathrm{op}} = 0.90 \pm 0.02$ and $\eta_{\mathrm{mm}} = 0.95 \pm 0.02$, giving a total homodyne efficiency of $\eta_{\mathrm{hd}} = 0.77 \pm 0.02$.

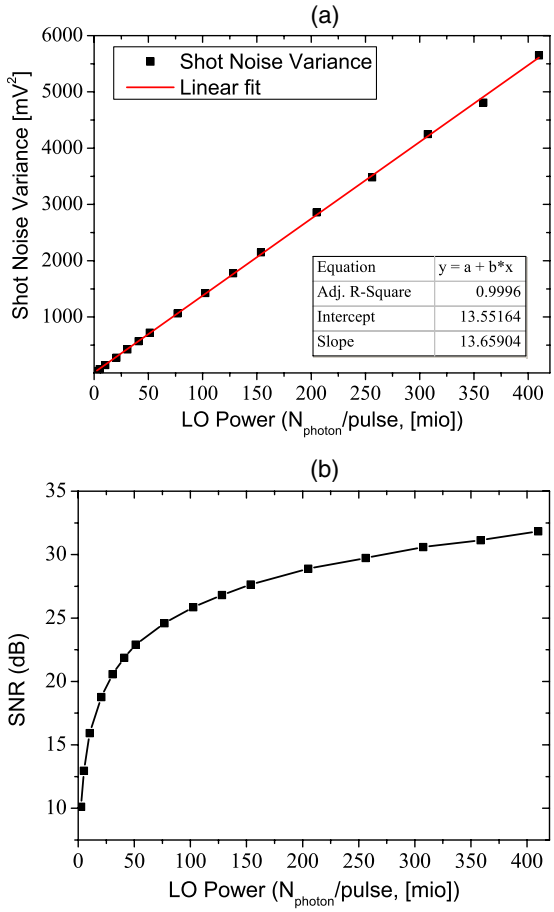

Fig. 5. (a) Quadrature variance measurement of the shot noise as a function of the LO power. (b) SNR of the shot noise variance as a function of the LO power. ([mio] stands for "million.")

D. Photon Subtraction

The reflected photons from ABS2 were detected by a fiber coupled APD (Perkin-Elmer SPCM-AQR-14-FC). Using this signal as a trigger, we conditionally prepared a photon-subtracted squeezed state. To reduce the effect of detector dark counts, the trigger signal for the homodyne measurement is derived by correlating the APD signal with the cavity dumper signal (see Fig. 2). By setting the coincidence window to 120 ns—corresponding to 1/10 of the total measurement window—we achieved a 10fold decrease in the detector dark counts, resulting in a dark count rate of $2.0 \pm 0.5\,s^{-1}$. To ensure that the APD detection events are spatially and spectrally matched with the optical mode of the LO it is necessary to employ filtering in the APD arm. The spectral filtering was carried out using a fiber-coupled tunable Fabry–Perot (FP) filter cavity (Micron Optics, FFP-TF-830-005). It was coupled via two 1.5 meter long single-mode fiber pigtails for spatial filtering. The bandwidth of the filter was 22 GHz corresponding to 0.05 nm, and the central wavelength could be tuned using a voltage supply. The total detection efficiency of the heralding channel was estimated to be about $10 \pm 5\%$ including the coupling efficiency to the fiber, the peak transmission of the FP filter, and the detection efficiency of the APD.

E. Gaussian Model for Estimation of Photon-Subtracted Squeezed State

In order to predict the performance of the photon-subtraction experiment, we derived a simple model [35,57,74]. The model takes into account various experimental imperfections, which could compromise the quality of the prepared output states. The analysis is broken into three parts. The first part is the generation of the squeezed state. The second is the tap-off on the asymmetric beamsplitter and projection onto the on–off click detector with a filter in front. Finally, the third part is the imperfect homodyne detector used for characterization. We choose to work with the Wigner quasi-probability distributions since they provide a convenient framework for such types of models. In the Wigner picture the vacuum state is given by a simple Gaussian distribution in the quadrature variables $\hat{X} = [x, p]^T$

$$W_0(\hat{X}) = \frac{e^{-x^2-p^2}}{\pi}. \tag{3}$$

A squeezed state can be written in the same way with the variables rescaled according to the quadrature variances V_{xp}

$$W_s(\hat{X}) = \frac{e^{-\frac{x^2}{V_x}-\frac{p^2}{V_p}}}{\pi\sqrt{V_x V_p}}, \tag{4}$$

where the Heisenberg uncertainty principle constrains the variances as $V_x V_p \geq 1$. The squeezed state is split on an asymmetric beamsplitter with a reflectivity R, and one part is measured using the positive operator value measure (POVM) element, $\hat{\Lambda} = \hat{1} - |0\rangle\langle 0|$ [75],

$$W_{\text{out}}(\hat{X}_1) = \frac{1}{2\pi}\int W(\hat{X}_1,\hat{X}_2)W_{\Lambda}(\hat{X}_2)\mathrm{d}\hat{X}_2, \tag{5}$$

where $W(\hat{X}_1,\hat{X}_2)$ is the Wigner function of the state after the asymmetric beamsplitter and $W_{\Lambda}(\hat{X}_2)$ is the Wigner function for the POVM element.

In Section 2.D, we described how a proper filtering in the heralding arm was necessary in order to ensure that identical modes were detected by the APD and the homodyne detector simultaneously. However, in practice, some false modes will be detected by the APD. This will be modeled by the modal purity parameter Ξ, and it describes the probability that the photon detected from the APD came from the targeted optical mode. The output from the system can then be expressed as follows:

$$W_{\text{out},\Xi}(\hat{X}) = \Xi W_{\text{out}}(\hat{X}) + (1-\Xi)W_s(\hat{X}), \tag{6}$$

where $W_s(\hat{X})$ is the state we see when the APD detections are uncorrelated with the optical mode used in the experiment.

3. EXPERIMENTAL RESULTS

A. Squeezed Vacuum

Using the data acquisition method as described in Section 2.C, the squeezed vacuum produced by the SPDC was characterized. The relative phase between the LO and the quantum state was scanned by a sawtooth modulation applied to a piezocrystal attached to a highly reflecting mirror placed in the LO arm. The sampling rate and acquisition time of the oscilloscope was set as 100 MS/s and 80 ms, then we acquired $\sim 65,200$ quadrature values in one run. The minimum and maximum quadrature variances of the squeezed pulses were measured as a function of pump power and the measured values are shown in Fig. 6.

Assuming a loss model, the squeezing and antisqueezing variances, $V_{\{\text{min,max}\}}$, can be fitted to a simple relation

$$V_{\{\text{min,max}\}} = \eta_{\text{tot}}(g_{\text{min}}, g_{\text{max}}) + (1-\eta_{\text{tot}})V_{\text{vac}}, \tag{7}$$

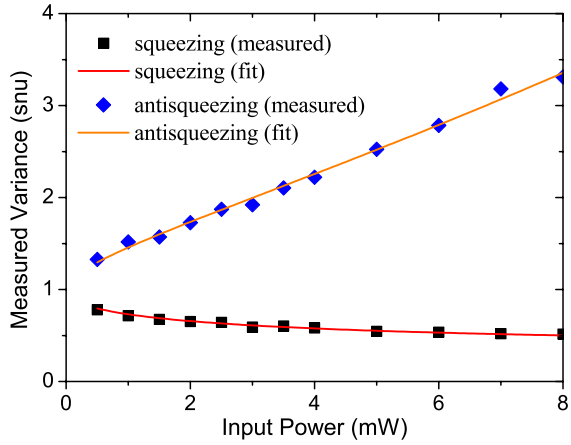

Fig. 6. Measured squeezing and antisqueezing variances as a function of the pump power. The blue diamonds are the measured maximum variances (antisqueezing), the black squares are the measured minimum variances (squeezing). The orange and red lines are the fittings according to Eq. (7), where $\eta_{\text{tot}} = 0.62 \pm 0.01$ are given.

where $g_{\{\text{min,max}\}}$ is the parametric gain, η_{tot} is the total detection efficiency, and V_{vac} is the quadrature variance of the vacuum state. By setting the parametric gain to the values found in Section 2.B, we find reasonable fits to both series of data for $\eta_{\text{tot}} = 0.62 \pm 0.01$, which is apparently lower than the experimentally accessed one of 0.77 (see Section 2.C). Part of the discrepancy is caused by the tap-off beamsplitter, which adds 8% loss to the squeezed states. The remaining discrepancy is about 12%, which we speculate to result from a mismatch between the temporal modes of the LO and the squeezed vacuum [64,76]. However, as this loss effect has not been carefully studied and localized, we will use $\eta = 0.77$ as the estimated detection efficiency to correct the experimental data for losses.

Using the experimental parameters in Fig. 6 as well as the formalism given in Section 2.E, the expected properties of the photon-subtraction squeezed state can be theoretically predicted. The estimated values for the fidelity to the odd cat state F_{odd}, its amplitude α_{odd}, and the negativity of its Wigner function at the origin $W(0,0)$, corresponding to the photon-subtraction squeezed states under four different pump power levels, are listed in Table 1 and Table 2 (corrected for detection losses).

It is clear that any one of the photon-subtracted squeezed states is expected to exhibit strong non-Gaussianity with relatively large negativities of the Wigner functions [37]. According to [77], the state prepared by conditionally subtracting a single photon from a squeezed vacuum state was non-Gaussian even when its Wigner function was positive at the origin.

B. Photon-Subtracted Squeezed Vacuum

Next, we prepared photon-subtracted squeezed states for different pump powers ranging from 2 to 8 mW. In this range, the

Table 1. Estimation of the Parameters Characterizing the Photon-Subtracted Squeezed State for Different Pump Power Levels[a]

P_p (mW)	F_{odd}	α	$W(0,0)$
2.0	0.64	0.87	−0.09
4.0	0.58	1.05	−0.06
6.0	0.55	1.20	−0.04
8.0	0.52	1.32	−0.03

[a]The predictions are based on the measured values for the squeezed vacuum states. In these estimates, we have set the mode match parameter Ξ to unity for all power levels.

Table 2. Estimation of the Parameters Characterizing the Photon-Subtracted Squeezed State for Different Pump Power Levels[a]

P_p (mW)	F_{odd}	α	$W(0,0)$
2.0	0.84	0.99	−0.21
4.0	0.74	1.18	−0.16
6.0	0.69	1.34	−0.13
8.0	0.63	1.45	−0.11

[a]After correcting for the homodyne detection losses of $1-\eta = 0.23$.

photon detection rate of the APD varied from 400 to 4000 s^{-1}. Each time a detection event from the APD was correlated with the sync signal from the laser, a trigger signal was derived and sent to the oscilloscope, as seen in Section 2.A. For every trigger signal, the digital oscilloscope sampled the homodyne signal for 1 μs with a sampling rate of 250 MS/s, making up a single measurement segment. Due to the limited memory of the oscilloscope, only 4000 data segments can be consecutively stored. The quadratures were extracted in the same way as for the squeezing measurement. During one measurement series the relative phase between the LO and the quantum state was scanned over a range of $0–3\pi$.

We used maximum likelihood estimation to reconstruct the prepared quantum state [78–80]. In order to reconstruct the quantum state, an estimation of the phase reference was required. Since the phase was scanned, we did not have a stable phase reference. In order to extract the phase information, the quadrature data was stored in bins of 100 quadratures and the variance of each bin was evaluated. The phase of bin i was initially assigned by comparing its variance to the

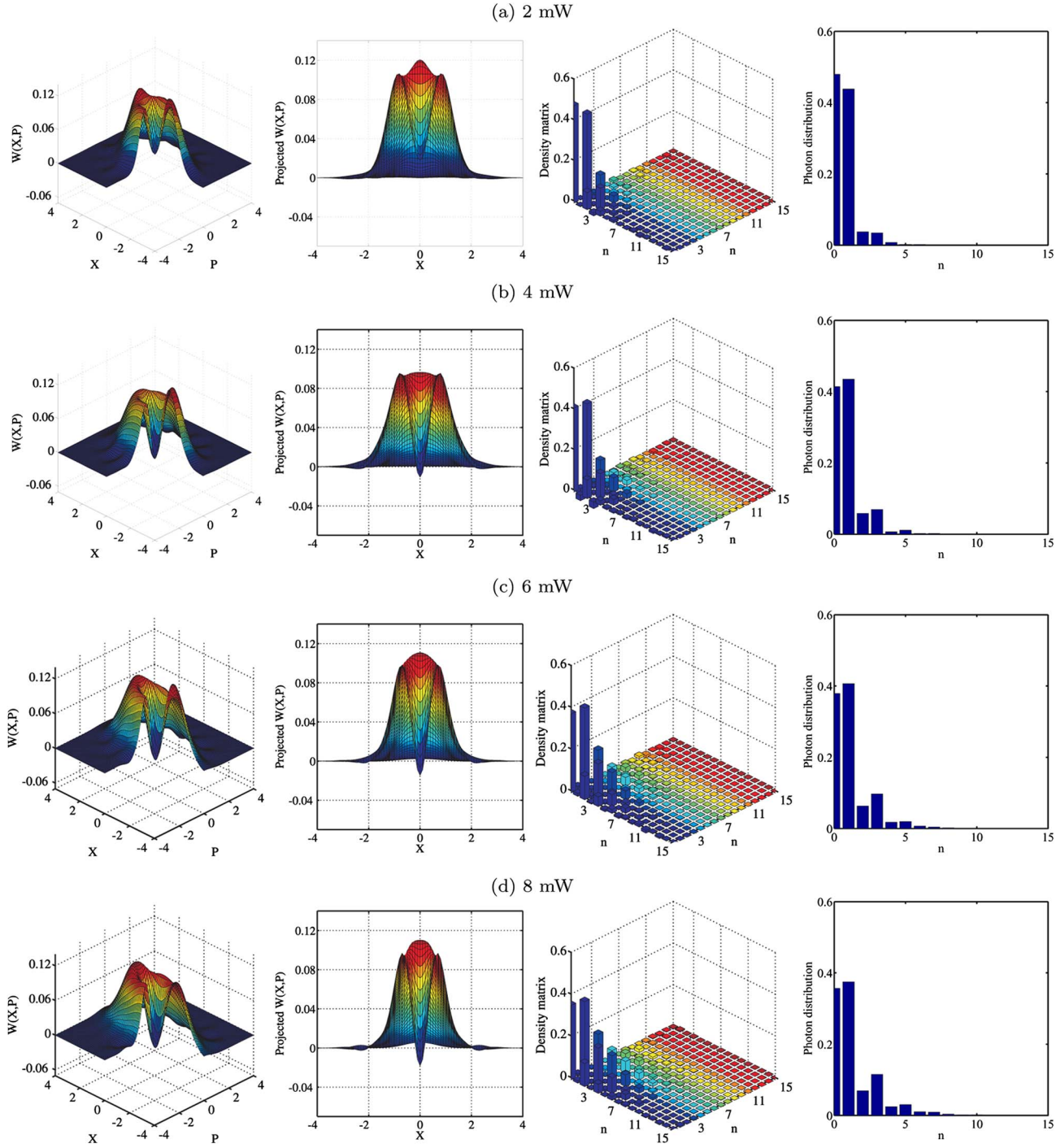

Fig. 7. Plot of the Wigner functions, the projected Wigner functions, the density matrices, and the photon distributions of the reconstructed states for pump powers from 2 to 8 mW. There are no corrections for losses in these plots.

minimum and maximum variances using the relation $V_i(\theta_i) = V_{\min}\cos^2\theta_i + V_{\max}\sin^2\theta_i$, where θ_i is the phase associated with bin i. Without loss of generality, the assigned phase was chosen between 0 and $\pi/2$. By using a saw tooth function to fit θ_i, the phase information for each measurement run was smoothly estimated. The phase-assigned quadrature files were then concatenated, and the entire batch of quadrature measurements was used for reconstruction. Based on the above algorithm, we reconstructed the density matrices and from those we calculated the Wigner quasi-probability distributions, see Fig. 7 (without loss-correction) and Fig. 8 (corrected for losses).

From Fig. 7 we see that the generated states are non-Gaussian and nonclassical. Moreover, it is evident that the Wigner functions become more squeezed as the pump power increases while the dip around the origin retains its structure. The dip attains a negative value for all realizations if the measurement results are corrected for losses, as seen in Fig. 8. The maximum measured negativity for the uncorrected data is $W(0,0) = -0.023$ which corresponds to a negativity of

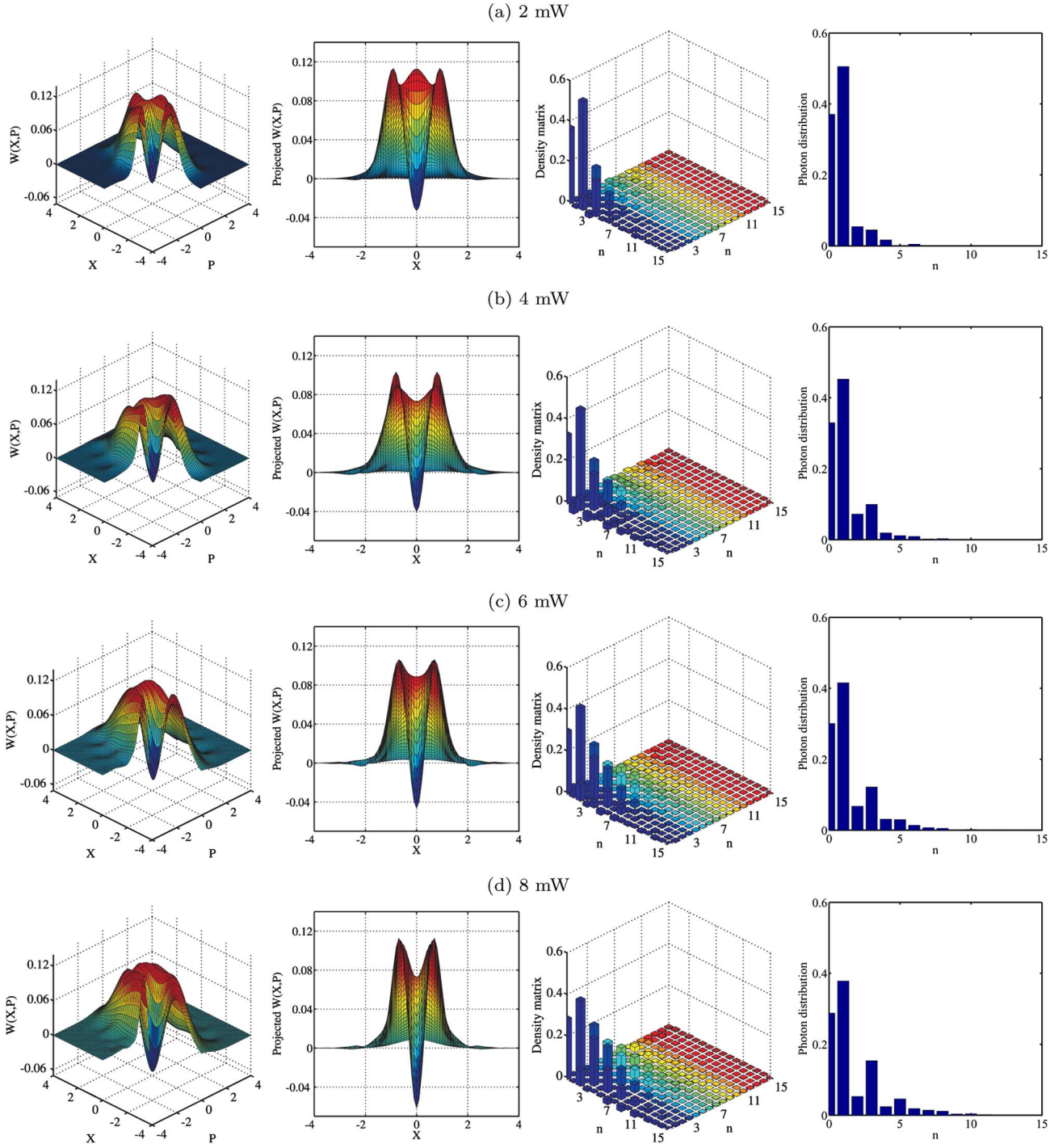

Fig. 8. Plot of the Wigner functions, the projected Wigner functions, the density matrices, and the photon distributions of the loss-corrected reconstructed states for pump powers from 2 to 8 mW.

Table 3. Parameters Characterizing the Prepared Photon-Subtracted Squeezed States

P_p (mW)	F_{odd}	α	$W(0,0)$	Ξ
.0	0.46	0.77	0.016	0.72
4.0	0.47	0.88	−0.011	0.86
6.0	0.49	1.08	−0.018	0.91
8.0	0.49	1.19	−0.023	0.96

Table 4. Parameters Characterizing the Prepared Photon-Subtracted Squeezed States after Correction for Imperfect Detection

P_p (mW)	F_{odd}	α	$W(0,0)$
.0	0.55	0.83	−0.033
4.0	0.53	1.01	−0.042
6.0	0.54	1.17	−0.050
8.0	0.56	1.32	−0.063

$W(0,0) = -0.063$ after loss correction. The fidelities between the experimentally produced states and the ideal cat states (maximized over the excitations α) are summarized in Table 3.

By comparing the results in Table 3 with the predictions in Table 1 we see that the fidelities, as well as the negativities, are generally smaller than predicted. The discrepancy, however, gets smaller at higher pump powers. This effect is caused by slow instabilities of the experimental setup which become significant for longer measurement runs as is the case for low pump powers where the run time is about 10 s (to acquire 4000 quadrature values). For high powers, however, the measurement time (1–2 s) is shorter and thus the influence of instabilities is less pronounced. The main source of instability is a mechanical drift of the filtering Fabry–Perot cavity which was not actively stabilized during the measurement. A drift of the cavity results in the detection by the APD of the frequency modes, which are different from the ones measured at the homodyne detector, which results in degradation of the performance. This corresponds to a lower value of the parameter Ξ in Eq. (6). To estimate values for the mode match parameter Ξ for the different power levels, we fit the theoretical predictions to the actual measurement results by using Ξ as a fitting parameter. The obtained values of Ξ for which the theoretical fidelities and Wigner function negativities match the experimental ones are shown in Table 3, which shows that the mode matching parameter is increasing for increasing pump powers.

Incorporating the generalized Bernoulli transformation into the maximum likelihood algorithm, the homodyne detection inefficiency can be corrected [80]. As mentioned above, we used the conservative estimate of the detection efficiency of 77% for the correction in order to avoid overestimating the negativities of the corrected Wigner functions. The Wigner functions after correction are displayed in Fig. 8, and the results for the fidelities, negativities, and sizes are summarized in Table 4.

4. CONCLUSION

We have presented the preparation of photon-subtracted squeezed states in a system based on picosecond pulsed laser pulses. It is based on generating a squeezed vacuum from SPDC in a PPKTP crystal followed by single photon subtraction, enabled by the reflection of a single photon on an asymmetric beamsplitter and its detection by the APD. Various states were produced with varying degree of squeezing. The resulting states were fully characterized by homodyne tomography with which the Wigner functions and density matrices were reconstructed. We found a maximum negativity of $W(0,0) = -0.023$ without any loss-corrections and $W(0,0) = -0.063$ after loss-correction. The negativity appeared to be largest for the largest degrees of squeezing. It is attributed to the shorter measurement time associated with larger squeezing and thus greater robustness to instabilities of the setup. To improve the results, the setup should be made more stable through miniaturization, faster measurements, and active control of some key parts of the experiment. Such improvements serve as an outlook for future experiments.

ACKNOWLEDGMENTS

The work was financed by the Danish Research Agency (Project No. FNU 09-072623). LAK acknowledges the A-STAR Investigatorship grant for the support of research visits to DTU. MJ also acknowledges support by the Operational Program Education for Competitiveness (Project No. CZ.1.07/2.3.00/20.0060) cofinanced by the European Social Fund and the Czech Ministry of Education.

REFERENCES

1. L. A. Wu, H. J. Kimble, J. Hall, and H. Wu, "Generation of squeezed states by parametric down conversion," Phys. Rev. Lett. **57**, 2520–2523 (1986).
2. H. Vahlbruch, M. Mehmet, S. Chelkowski, B. Hage, A. Franzen, N. Lastzka, S. Gossler, K. Danzmann, and R. Schnabel, "Observation of squeezed light with 10-dB quantum-noise reduction," Phys. Rev. Lett. **100**, 033602 (2008).
3. Y. Takeno, M. Yukawa, H. Yonezawa, and A. Furusawa, "Observation of −9 dB quadrature squeezing with improvement of phase stability in homodyne measurement," Opt. Express **15**, 4321–4327 (2007).
4. R. Dong, J. Heersink, J. F. Corney, P. D. Drummond, U. L. Andersen, and G. Leuchs, "Experimental evidence for Raman-induced limits to efficient squeezing in optical fibers," Opt. Lett. **33**, 116–118 (2008).
5. M. G. A. Paris, "Displacement operator by beam splitter," Phys. Lett. **217**, 78–80 (1996).
6. S. Lloyd, "Coherent quantum feedback," Phys. Rev. A **62**, 022108 (2000).
7. S. Scheel, W. Munro, J. Eisert, K. Nemoto, and P. Kok, "Feedforward and its role in conditional linear optical quantum dynamics," Phys. Rev. A **73**, 034301 (2006).
8. H. M. Wiseman and G. J. Milburn, "Quantum theory of optical feedback via homodyne detection," Phys. Rev. Lett. **70**, 548–551 (1993).
9. A. Furusawa, S. L. Braunstein, J. L. Sørensen, C. A. Fuchs, H. J. Kimble, and E. S. Polzik, "Unconditional quantum teleportation," Science **282**, 706–709 (1998).
10. F. Grosshans, G. V. Assche, J. Wenger, R. Brouri, N. J. Cerf, and P. Grangier, "Quantum key distribution using Gaussian-modulated coherent states," Nature (London) **421**, 238–241 (2003).
11. U. L. Andersen, V. Josse, and G. Leuchs, "Unconditional quantum cloning of coherent states with linear optics," Phys. Rev. Lett. **94**, 240503 (2005).
12. A. M. Lance, T. Symul, W. P. Bowen, B. Sanders, T. Tyc, T. C. Ralph, and P. K. Lam, "Continuous-variable quantum-state sharing via quantum disentanglement," Phys. Rev. Lett. **71**, 033814 (2005).

13. R. Ukai, N. Iwata, Y. Shimokawa, S. Armstrong, A. Politi, J. Yoshikawa, P. V. Loock, and A. Furusawa, "Demonstration of unconditional one-way quantum computations for continuous variables," Phys. Rev. Lett. **106**, 240504 (2011).
14. C. Weedbrook, S. Pirandola, R. Garca-Patrón, N. J. Cerf, T. C. Ralph, J. H. Shapiro, and S. Lloyd, "Gaussian quantum information," Rev. Mod. Phys. **84**, 621 (2012).
15. J. Eisert, S. Scheel, and M. Plenio, "Distilling Gaussian states with Gaussian operations is impossible," Phys. Rev. Lett. **89**, 137903 (2002).
16. J. Fiurášek, "Gaussian transformations and distillation of entangled Gaussian states," Phys. Rev. Lett. **89**, 137904 (2002).
17. G. Giedke and J. I. Cirac, "Characterization of Gaussian operations and distillation of Gaussian states," Phys. Rev. A **66**, 032316 (2002).
18. J. Niset, J. Fiurášek, and N. J. Cerf, "No-go theorem for Gaussian quantum error correction," Phys. Rev. Lett. **102**, 120501 (2009).
19. S. Lloyd and S. L. Braunstein, "Quantum computation over continuous variables," Phys. Rev. Lett. **82**, 1784–1787 (1999).
20. M. Ohliger, K. Kieling, and J. Eisert, "Limitations of quantum computing with Gaussian cluster states," Phys. Rev. A **82**, 042336 (2010).
21. L. Magnin, F. Magniez, A. Leverrier, and N. J. Cerf, "Strong no-go theorem for Gaussian quantum bit commitment," Phys. Rev. A **81**, 010302 (2010).
22. J. Bell, *Speakable and Unspeakable in Quantum Mechanics* (Cambridge University, 1987).
23. N. Menicucci, P. van Loock, M. Gu, C. Weedbrook, T. C. Ralph, and M. A. Nielsen, "Universal quantum computation with continuous-variable cluster states," Phys. Rev. Lett. **97**, 110501 (2006).
24. A. Ourjoumtsev, R. Tualle-Brouri, P. Grangier, and A. Dantan, "Increasing entanglement between Gaussian states by coherent photon subtraction," Phys. Rev. Lett. **98**, 030502 (2007).
25. H. Takahashi, J. S. Neergaard-Nielsen, M. Takeuchi, M. Takeoka, K. Hayasaka, A. Furusawa, and M. Sasaki, "Entanglement distillation from Gaussian input states," Nat. Photonics **4**, 178–181 (2010).
26. M. Lassen, M. Sabuncu, A. Huck, J. Niset, G. Leuchs, N. J. Cerf, and U. L. Andersen, "Quantum optical coherence can survive photon losses using a continuous-variable quantum erasure-correcting code," Nat. Photonics **4**, 700–705 (2010).
27. T. C. Ralph, A. Gilchrist, G. J. Milburn, W. J. Munro, and S. Glancy, "Quantum computation with optical coherent states," Phys. Rev. A **68**, 042319 (2003).
28. A. P. Lund, H. Jeong, T. C. Ralph, and M. S. Kim, "Conditional production of superpositions of coherent states with inefficient photon detection," Phys. Rev. A **70**, 020101 (2004).
29. A. Gilchrist, K. Nemoto, W. Munro, T. C. Ralph, S. Glancy, S. L. Braunstein, and G. J. Milburn, "Schrödinger cats and their power for quantum information processing," J. Opt. B **6**, 828–833 (2004).
30. T. C. Ralph, "Quantum error correction of continuous-variable states against Gaussian noise," Phys. Rev. A **84**, 022309 (2011).
31. R. Garca-Patrón, J. Fiurášek, N. J. Cerf, J. Wenger, R. Tualle-Brouri, and P. Grangier, "Proposal for a loophole-free bell test using homodyne detection," Phys. Rev. Lett. **93**, 130409 (2004).
32. A. Mandilara and N. J. Cerf, "Quantum bit commitment under Gaussian constraints," Phys. Rev. A **85**, 062310 (2012).
33. A. I. Lvovsky, H. Hansen, T. Aichele, O. Benson, J. Mlynek, and S. Schiller, "Quantum state reconstruction of the single-photon fock state," Phys. Rev. Lett. **87**, 050402 (2001).
34. T. Aichele, A. I. Lvovsky, and S. Schiller, "Optical mode characterization of single photons prepared by means of conditional measurements on a biphoton state," Eur. Phys. J. D **18**, 237–245 (2002).
35. A. Ourjoumtsev, R. Tualle-Brouri, and P. Grangier, "Quantum homodyne tomography of a two-photon Fock state," Phys. Rev. Lett. **96**, 213601 (2006).
36. S. R. Huisman, N. Jain, S. A. Babichev, F. Vewinger, A. N. Zhang, S. H. Youn, and A. I. Lvovsky, "Instant single-photon Fock state tomography," Opt. Lett. **34**, 2739–2741 (2009).
37. J. Wenger, R. Tualle-Brouri, and P. Grangier, "Non-Gaussian statistics from individual pulses of squeezed light," Phys. Rev. Lett. **92**, 153601 (2004).
38. M. Cooper, L. J. Wright, C. Söller, and B. J. Smith, "Experimental generation of multi-photon Fock states," Opt. Express **21**, 5309–5317 (2013).
39. K. Laiho, K. N. Cassemiro, D. Gross, and C. Silberhorn, "Probing the negative Wigner function of a pulsed single photon point by point," Phys. Rev. Lett. **105**, 253603 (2010).
40. Y. Miwa, J. Yoshikawa, N. Iwata, M. Endo, P. Marek, R. Filip, P. van Loock, and A. Furusawa, "Unconditional conversion between a single-photon state and a coherent-state superposition via squeezing operation," Quantum Electronics and Laser Science Conference, San Jose, California, United States, May 6–11, 2012.
41. H. Jeong, M. S. Kim, and J. Lee, "Quantum-information processing for a coherent superposition state via a mixed entangled coherent channel," Phys. Rev. A **64**, 052308 (2001).
42. P. Marek and M. S. Kim, "Suitability of the approximate superposition of squeezed coherent states for various quantum protocols," Phys. Rev. A **78**, 022309 (2008).
43. H. Jeong and M. S. Kim, "Efficient quantum computation using coherent states," Phys. Rev. A **65**, 042305 (2002).
44. P. Marek and J. Fiurášek, "Elementary gates for quantum information with superposed coherent states," Phys. Rev. A **82**, 014304 (2010).
45. A. Tipsmark, R. Dong, A. Laghaout, P. Marek, M. Ježek, and U. L. Andersen, "Experimental demonstration of a Hadamard gate for coherent state qubits," Phys. Rev. A **84**, 050301 (2011).
46. R. Blandino, F. Ferreyrol, M. Barbieri, P. Grangier, and R. Tualle-Brouri, "Characterization of a π-phase shift quantum gate for coherent-state qubits," New J. Phys. **14**, 013017 (2012).
47. D. Wilson, H. Jeong, and M. S. Kim, "Quantum nonlocality for a mixed entangled coherent state," J. Mod. Opt. **49**, 851–864 (2002), Special Issue for QEP 15.
48. H. Jeong, W. Son, M. S. Kim, D. Ahn, and C. Brukner, "Quantum nonlocality test continuous-variable states with dichotomic observable," Phys. Rev. A **67**, 012106 (2003).
49. H. Jeong, "Testing Bell inequalities with photon-subtracted Gaussian states," Phys. Rev. A **78**, 042101 (2008).
50. M. Dakna, T. Anhut, T. Opatrný, L. Knöll, and D. G. Welsch, "Generating Schrödinger-cat-like states by means of conditional measurements on a beam splitter," Phys. Rev. A **55**, 3184–3194 (1997).
51. P. Marek, H. Jeong, and M. S. Kim, "Generating "squeezed" superpositions of coherent states using photon addition and subtraction," Phys. Rev. A **78**, 063811 (2008).
52. H. Takahashi, K. Wakui, S. Suzuki, M. Takeoka, K. Hayasaka, A. Furusawa, and M. Sasaki, "Generation of large-amplitude coherent-state superposition via ancilla-assisted photon subtraction," Phys. Rev. Lett. **101**, 233605 (2008).
53. J. B. Brask, R. Chaves, and N. Brunner, "Testing nonlocality of a single photon without a shared reference frame," Phys. Rev. A **88**, 012111 (2013).
54. A. Laghaout, J. S. Neergaard-Nielsen, I. Rigas, C. Kragh, A. Tipsmark, and U. L. Andersen, "Amplification of realistic Schrödinger-cat-state-like states by homodyne heralding," Phys. Rev. A **87**, 043826 (2013).
55. A. Ourjoumtsev, R. Tualle-Brouri, and P. Grangier, "Generating optical Schrödinger kittens for quantum information processing," Science **312**, 83–86 (2006).
56. A. Ourjoumtsev, H. Jeong, R. Tualle-Brouri, and P. Grangier, "Generation of optical "Schrödinger cats" from photon number stataes," Nature **448**, 784–786 (2007).
57. J. S. Neergaard-Nielsen, B. Melholt Nielsen, C. Hettich, K. Mølmer, and E. S. Polzik, "Generation of a superposition of odd photon number states for quantum information networks," Phys. Rev. Lett. **97**, 083604 (2006).
58. K. Wakui, H. Takahashi, A. Furusawa, and M. Sasaki, "Photon subtracted squeezed states generated with periodically poled $KTiOPO_4$," Opt. Express **15**, 3568–3574 (2007).
59. T. Gerrits, S. Glancy, T. S. Clement, B. Calkins, A. E. Lita, A. J. Miller, A. L. Migdall, S. W. Nam, R. P. Mirin, and E. Knill, "Generation of optical coherent state superpositions by number-resolved photon subtraction from squeezed vacuum," Phys. Rev. A **82**, 031802 (2010).
60. N. Namekata, Y. Takahashi, G. Fujii, D. Fukuda, S. Kurimura, and S. Inoue, "Non-Gaussian operation based on photon

subtraction using a photon-number-resolving detector at a telecommunications wavelength," Nat. Photonics **4**, 655–660 (2010).
61. J. S. Neergaard-Nielsen, M. Takeuchi, K. Wakui, H. Takahashi, K. Hayasaka, M. Takeoka, and M. Sasaki, "Optical continuous-variable qubit," Phys. Rev. Lett. **105**, 053602 (2010).
62. N. Lee, H. Benichi, Y. Takeno, S. Takeda, J. Webb, E. Huntington, and A. Furusawa, "Teleportation of nonclassical wave packets of light," Science **332**, 330–333 (2011).
63. C. Kim, R. D. Li, and P. Kumar, "Deamplification response of a traveling-wave phase-sensitive optical parametric amplifier," Opt. Lett. **19**, 132–134 (1994).
64. G. D. Boyd and D. A. Kleinman, "Parametric interaction of focused Gaussian light beams," J. Appl. Phys. **39**, 3597–3639 (1968).
65. J. Wenger, R. Tualle-Brouri, and P. Grangier, "Pulsed homodyne measurements of femtosecond squeezed pulses generated by single-pass parametric deamplification," Opt. Lett. **29**, 1267–1269 (2004).
66. A. La Porta and R. Slusher, "Squeezing limits at high parametric gains," Phys. Rev. A **44**, 2013–2022 (1991).
67. A. I. Lvovsky, "Continuous-variable optical quantum-state tomography," Rev. Mod. Phys. **81**, 299–332 (2009).
68. H. Hansen, T. Aichele, C. Hettich, P. Lodahl, A. I. Lvovsky, J. Mlynek, and S. Schiller, "Ultrasensitive pulsed, balanced homodyne detector: application to time-domain quantum measurements," Opt. Lett. **26**, 1714–1716 (2001).
69. J. P. Gordon, W. Louisel, and L. Walker, "Quantum fluctuations and noise in parametric processes. II," Phys. Rev. Lett. **129**, 481–485 (1963).
70. W. Wagner and R. Hellwarth, "Quantum noise in a parametric amplifier with lossy modes," Phys. Rev. A **133**, A915–A920 (1964).
71. R. Byer and S. Harris, "Power and bandwidth of spontaneous parametric emission," Phys. Rev. **168**, 1064–1068 (1968).
72. T. Hirano, K. Kotani, T. Ishibashi, S. Okude, and T. Kuwamoto, "3 dB squeezing by single-pass parametric amplification in a periodically poled $KTiOPO_4$ crystal," Opt. Lett. **30**, 1722–1724 (2005).
73. J. Appel, D. Hoffman, E. Figueroa, and A. I. Lvovsky, "Electronic noise in optical homodyne tomography," Phys. Rev. A **75**, 035802 (2007).
74. R. Tualle-Brouri, A. Ourjoumtsev, A. Dantan, P. Grangier, M. Wubs, and A. Sørensen, "Multimode model for projective photon-counting measurements," Phys. Rev. A **80**, 013806 (2009).
75. S. Suzuki, K. Tsujino, F. Kannari, and M. Sasaki, "Analysis on generation schemes of Schrödinger cat-like states under experimental imperfections," Opt. Commun. **259**, 758–764 (2006).
76. R. Demkowicz-Dobrzanski, U. Dorner, B. J. Smith, J. S. Lundeen, W. Wasilewski, K. Banaszek, and I. A. Walmsley, "Quantum phase estimation with lossy interferometers," Phys. Rev. A **80**, 013825 (2009).
77. M. Ježek, A. Tipsmark, R. Dong, J. Fiurášek, L. Mišta, Jr., R. Filip, and U. L. Andersen, "Experimental test of the strongly nonclassical character of a noisy squeezed single-photon state," Phys. Rev. A **86**, 043813 (2012).
78. Z. Hradil, "Quantum-state estimation," Phys. Rev. A **55**, R1561–R1564 (1997).
79. M. Ježek, J. Fiurášek, and Z. Hradil, "Quantum inference of states and processes," Phys. Rev. A **68**, 012305 (2003).
80. A. I. Lvovsky, "Iterative maximum-likelihood reconstruction in quantum homodyne tomography," J. Opt. B **6**, S556–S559 (2004).